

Dopant Induced Modification of Active Site Structure and Surface Bonding Mode for High Performance Nanocatalysts: CO Oxidation on Capping-free (110)-Oriented CeO₂:Ln (Ln = La–Lu) Nanowires

Jun Ke,[†] Jia-Wen Xiao,^{†,‡} Wei Zhu,^{†,‡} Haichao Liu,^{‡,*} Rui Si,[§] Ya-Wen Zhang,^{†,*} and Chun-Hua Yan^{†,*}

[†] Beijing National Laboratory for Molecular Sciences, State Key Laboratory of Rare Earth Materials Chemistry and Applications, PKU-HKU Joint Laboratory in Rare Earth Materials and Bioinorganic Chemistry, College of Chemistry and Molecular Engineering, Peking University, Beijing 100871, China.

[‡] Beijing National Laboratory for Molecular Sciences, State Key Laboratory for Structural Chemistry of Stable and Unstable Species, College of Chemistry and Molecular Engineering, Peking University, Beijing 100871, China.

[§] Shanghai Synchrotron Radiation Facility, Shanghai Institute of Applied Physics, Chinese Academy of Sciences, Shanghai 201204, China.

* Correspondence to: ywzhang@pku.edu.cn, hcliu@pku.edu.cn, yan@pku.edu.cn.

[‡] These authors contributed equally to this work.

Supplementary Data

Table S1. Lattice parameter, composition, and size of CeO₂:Ln nanowires.

Sample	^a Lattice parameter a / Å	Ln / atom%		^c Ce ³⁺ / atom%	Length / μm	Width / nm
		ICP-AES	^b XPS			
CeO ₂	5.43(7)	/	/	8	1–3	20–60
CeO ₂ :La	5.46(4)	10	10	undetected	1–5	25–60
CeO ₂ :Pr	5.44(5)	10	11	undetected	1–5	25–60
CeO ₂ :Nd	5.42(9)	10	11	undetected	1–5	25–60
CeO ₂ :Sm	5.43(6)	10	11	undetected	1–5	20–50
CeO ₂ :Eu	5.44(0)	10	12	undetected	1–4	20–50
CeO ₂ :Gd	5.43(2)	11	13	undetected	1–4	15–30
CeO ₂ :Dy	5.42(9)	10	10	undetected	0.1–0.5	10–20
CeO ₂ :Ho	5.42(3)	11	10	undetected	0.1–0.5	10–20
CeO ₂ :Er	5.41(8)	10	11	undetected	0.1–0.5	10–20
CeO ₂ :Tm	5.41(2)	10	9	undetected	0.05–0.2	5–15
CeO ₂ :Yb	5.40(7)	11	9	undetected	0.05–0.2	5–15
CeO ₂ :Lu	5.40(8)	11	8	undetected	0.05–0.2	5–15

^a 2θ correction and cell dimension calculation were performed using LAPOD code with least-squares refinement (Ref. S1 and S2). Uncertainty of the calculation was about $\pm 0.1\%$.

^b Background excluding, curve fitting, and peak area integration were performed using CasaXPS v2.3.15 software. Amounts of Ln and Ce were obtained from the peak area (A) of Ce 3d, La–Sm 3d, and Eu–Lu 4d spectra. The inelastic mean free path was estimated to be 10–29 Å from Ref. S3 ($h\nu = 1486.6$ eV, kinetic energy = ~ 400 –1350 eV). The doping ratio of Ln atoms at surface levels was calculated through the following equation:

$$\text{Ln \%} = \frac{A(\text{Ln}) \div S(\text{Ln})}{A(\text{Ln}) \div S(\text{Ln}) + A(\text{Ce}) \div S(\text{Ce})}$$

wherein, S is the relative sensitivity factor. Uncertainty for the fitting and measurements was estimated to be about $\pm 30\%$.

^c Ce 3d spectra of the samples were fitted as the linear combination of Ce(III) and Ce(IV) 3d spectra with the reported method (Ref. S4). See Figure S3b–d for the fitting.

Table S2. BET surface area and catalytic performance of CeO₂:Ln nanowires.

Sample	BET surface area / m ² ·g ⁻¹	T_{50} / °C	Specific reaction rate at 200 °C		TOF at 200 °C / s ⁻¹
			per unit weight of catalyst / mmol·h ⁻¹ ·g ⁻¹	per unit surface area / μmol·h ⁻¹ ·m ⁻²	
CeO ₂	39	350	0.11	2.8	4.1×10 ⁻⁵
CeO ₂ :La	43	322	0.33	7.7	1.3×10 ⁻⁴
CeO ₂ :Pr	43	334	0.10	2.3	4.0×10 ⁻⁵
CeO ₂ :Nd	44	252	1.38	31.4	5.4×10 ⁻⁴
CeO ₂ :Sm	44	260	1.34	30.5	5.3×10 ⁻⁴
CeO ₂ :Eu	34	294	0.60	17.6	3.1×10 ⁻⁴
CeO ₂ :Gd	35	298	0.73	20.9	3.6×10 ⁻⁴
CeO ₂ :Dy	60	315	0.41	6.8	1.2×10 ⁻⁴
CeO ₂ :Ho	70	308	0.46	6.6	1.1×10 ⁻⁴
CeO ₂ :Er	72	305	0.44	6.1	1.1×10 ⁻⁴
CeO ₂ :Tm	84	302	0.47	5.6	9.8×10 ⁻⁵
CeO ₂ :Yb	71	313	0.40	5.6	9.7×10 ⁻⁵
CeO ₂ :Lu	82	306	0.43	5.2	1.4×10 ⁻⁴

Table S3. EXAFS parameters for CeO₂:Ln nanowires.^a

Sample	Shell	R / Å	N	σ^2 / Å ²	ΔE_0 / eV
CeO ₂	Ce–O	2.34±0.01	6.3±0.4		
CeO ₂ :La	Ce–O	2.34±0.01	6.6±0.4		
CeO ₂ :Pr	Ce–O	2.34±0.01	6.5±0.5		
CeO ₂ :Nd	Ce–O	2.33±0.01	6.0±0.4	0.009±0.001	0.2±0.4
CeO ₂ :Gd	Ce–O	2.33±0.01	6.1±0.5		
CeO ₂ :Ho	Ce–O	2.34±0.01	6.3±0.5		
CeO ₂ :Lu	Ce–O	2.35±0.01	6.1±0.4		
CeO ₂ :Gd	Gd–O	2.37±0.02	8.5±1.6	0.008±0.004	6.0±1.3
CeO ₂ :Ho	Ho–O	2.34±0.01	6.9±0.9	0.007±0.003	6.7±0.9
CeO ₂ :Lu	Lu–O	2.33±0.01	7.4±0.7	0.009±0.002	7.0±0.7

^a N , coordination number; R , interatomic distance between absorber and backscatter atoms; σ^2 , Debye–Waller-type factor; ΔE_0 , difference between the zero kinetic energy of the sample and that of the model used in the fitting. Athena and Artemis codes were used to extract the data and fit the curve with reported model (Ref. S5), respectively. Fitting of the first shell was performed in real space with $\Delta k = 2\text{--}9 \text{ \AA}^{-1}$ and $\Delta R = 1.2\text{--}2.5 \text{ \AA}$ for Ce (k^2 weighted), and with $\Delta k = 2\text{--}9 \text{ \AA}^{-1}$ and $\Delta R = 1.5\text{--}2.7 \text{ \AA}$ for Ln (k^3 weighted). S_0^2 was defined as 1 for Ce, Gd, Ho, and Lu. See Figure S7 for fitting curves.

Table S4. Surface Ln proportion and Ce³⁺ percentage for CeO₂:Ln nanowires after catalytic tests.

Sample	Ln / atom%	Ce ³⁺ / atom%	Sample	Ln / atom%	Ce ³⁺ / atom%
CeO ₂	/	undetected	CeO ₂ :Dy	10	undetected
CeO ₂ :La	10	undetected	CeO ₂ :Ho	9	undetected
CeO ₂ :Pr	11	undetected	CeO ₂ :Er	9	undetected
CeO ₂ :Nd	12	undetected	CeO ₂ :Tm	9	undetected
CeO ₂ :Sm	12	undetected	CeO ₂ :Yb	9	undetected
CeO ₂ :Eu	10	undetected	CeO ₂ :Lu	9	undetected
CeO ₂ :Gd	13	undetected			

Table S5. Oxygen vacancy formation energy on (110) surface exposed Ln doped CeO₂ with surface hydroxyl.^a

Dopant	E_V / eV	
	NN site	NNN site
undoped	1.74	1.46
La	0.35	0.12
Nd	0.31	0.06
Gd	0.18	0.37
Ho	0.34	0.52
Lu	0.25	0.58
Pr	0.25	0.40

^a One oxygen at NN site in Figure 4 in the *Article* was replaced by a hydroxyl. Oxygen vacancy formation energy at its most adjacent NN site and NNN site was calculated. The variation trend of E_V along Ln dopants was not similar to that obtained from the H₂-TPR analysis, indicating that hydroxyls only had very limited influence on the oxygen release tendency. Considering that hydroxyls might turn into bicarbonates and became hindrance effect for CO to approach the ceria surface (Ref. S6), hydroxyls were probably not suitable sites in pathway I.

Table S6. Oxygen vacancy formation energy and average interatomic distance for (110) surface exposed Ln doped CeO₂.

Dopant	^a Ionic radius of Ln ³⁺ / pm	E_V / eV		$R(\text{Ce-O})$	$R(\text{Ln-O})$	$R(\text{Ce-O})$	$R(\text{Ln-O})$
		NN site	NNN site	in all levels / pm	in all levels / pm	in surface level / pm	in surface level / pm
undoped	/	1.54		235	/	230	/
La	116	0.21	0.18	235	243	230	244
Nd	110.9	0.29	0.23	235	240	230	239
Gd	105.3	0.39	0.41	235	236	230	232
Ho	101.5	0.37	0.54	234	234	230	228
Lu	97.7	0.22	0.27	235	232	230	224
Pr	112.6	0.07	-0.15	235	235	230	230

^a Shannon ionic radius with coordination number of eight taken from Ref. S7. Ionic radius of Pr⁴⁺ and Ce⁴⁺ with coordination number of eight is 96 pm and 97 pm, respectively.

Table S7. V_O formation energy for (110) surface exposed CeO_2 with Ln dopants in surface level.^a

Dopant	Ionic radius of Ln^{3+} / pm	E_V / eV		E_V / eV (U on O 2p) ^b	
		NN site	NNN site	NN site	NNN site
undoped	/	1.54	/	0.91	/
La	116	0.52	0.17	0.65	0.25
Nd	110.9	0.48	0.28	0.62	0.29
Gd	105.3	0.47	0.28	0.49	0.35
Ho	101.5	0.34	0.33	0.42	0.39
Lu	97.7	0.21	0.41	0.32	0.45

^a One Ce at the surface level was replaced by an Ln dopant in $4 \times 4 \times 5$ ceria supercell with (110) surface. In this model, the doping ratio was 1.25%.

^b In some studies (Ref. S8 and S9), $U = 7$ eV was added on O 2p orbitals to simulate $[Ln^+-O^-]$ defect centers from non-equivalent doping. Variation trend for E_V at both NN site and NNN site was the same no matter whether $U = 7$ eV was added on O 2p orbitals or not.

Table S8. Proportion of peak area for each peak in XPS O 1s spectra of CeO_2 :Ln nanowires.^a

Sample	Peak area percentage / %		
	528.8 eV	531.0 eV	533.3 eV
CeO_2	53	45	3
CeO_2 :La	55	35	10
CeO_2 :Nd	54	38	8
CeO_2 :Gd	58	35	7
CeO_2 :Ho	55	39	6
CeO_2 :Lu	57	38	5

^a See Figure S3e for O 1s spectra and peak fitting. The peak at 529 eV represented lattice oxygen ions. The peak at 531 eV might be due to adsorbed oxygen, oxygen vacancy, hydroxide ions, or carbonates from CO_2 adsorption in air (Ref. S10 and S11). The peak at 533 eV might be assigned to surface bonded water or hydroxyls (Ref. S12 and S13). Its proportion had a decreasing trend for La–Lu doped samples. It might be attributed to the decreasing ionic potential of Ln^{3+} dopants along the Ln series, leading to the increasing trend for CeO_2 :Ln to be hydrated.

Table S9. Assignments of surface species in IR spectra.^a

Species	Wavenumber / cm^{-1}	
	Values in Literatures	Values in this work
Unidentate carbonates	1454, 1348, 1062, 854 (Ref. S5)	1454, 1378, 864
Bidentate carbonates	1562, 1286, 1028, 854 (Ref. S5)	1577, 1286, 1064, 864
Bicarbonates	1670-1695, 1310-1338, 650-970 (Ref. S14)	1644, 1378, 1216, 911
Inorganic carboxylates	1510, 1310 (Ref. S5)	1495
Bridged carbonates	1728, 1396, 1219, 1132 (Ref. S5)	1708, 1421, 1238
Formates	2939, 2848, 1576, 1550, 1371 (Ref. S15)	2848, 1566, 1372

^a The differences between the values observed in this work and those in literatures were probably due to the altered texture properties (such as shape, surface state, size and size distributions) of the samples led by different preparation methods.

Table S10. Ratio of each pair of absorbance at 1454 cm⁻¹ (unidentate carbonates), 1577 cm⁻¹ (bidentate carbonates), and 1644 cm⁻¹ (bicarbonates) from IR spectra.

Dopant	$A(1454\text{ cm}^{-1})/A(1644\text{ cm}^{-1})$	$A(1577\text{ cm}^{-1})/A(1644\text{ cm}^{-1})$	$A(1454\text{ cm}^{-1})/A(1577\text{ cm}^{-1})$
Pr	0.10	0.12	0.87
undoped	0.10	0.12	0.83
La	0.11	0.028	3.9
Nd	0.20	0.057	3.5
Gd	0.10	0.10	1.0
Ho	0.043	0.091	0.47
Lu	0.055	0.11	0.51

Table S11. CO adsorption energy and unidentate carbonate conversion energy for (110) surface exposed CeO₂ with Ln dopants in all levels.

Dopant	Ionic radius of Ln ³⁺ / pm	$E_{\text{ads}} / \text{eV}$	$\Delta E(\text{I})^{\text{a}} / \text{eV}$	$\Delta E(\text{II})^{\text{b}} / \text{eV}$
undoped	/	-3.69	-0.11	0.22
La	116	-4.62	-0.14	0.22
Nd	110.9	-4.63	-0.15	0.26
Gd	105.3	-4.59	-0.16	0.34
Ho	101.5	-4.60	-0.14	0.42
Lu	97.7	-4.64	-0.18	0.54
Pr	112.6	-4.55	0.67	-0.16

^a $\Delta E(\text{I}) = E(\text{CeO}_2 \text{ with unidentate carbonate I}) - E(\text{CeO}_2 \text{ with bidentate carbonate})$.

^b $\Delta E(\text{II}) = E(\text{CeO}_2 \text{ with unidentate carbonate II}) - E(\text{CeO}_2 \text{ with unidentate carbonate I}) - 0.5 E(\text{O}_2)$.

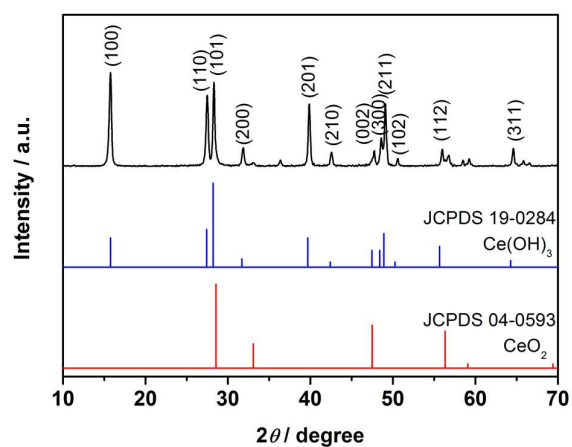


Figure S1. XRD patterns of the intermediate during the synthesis of CeO_2 nanowires, indicating the main composition of the intermediate is $\text{Ce}(\text{OH})_3$ in hexagonal structure.

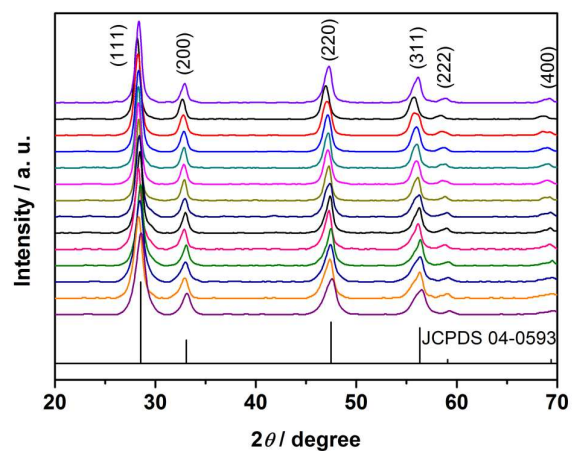


Figure S2. XRD patterns of the as-prepared $\text{CeO}_2:\text{Ln}$ nanowires. From the top to the bottom, each pattern refers to undoped, La, Pr, Nd, and Sm–Lu doped CeO_2 nanowires, respectively.

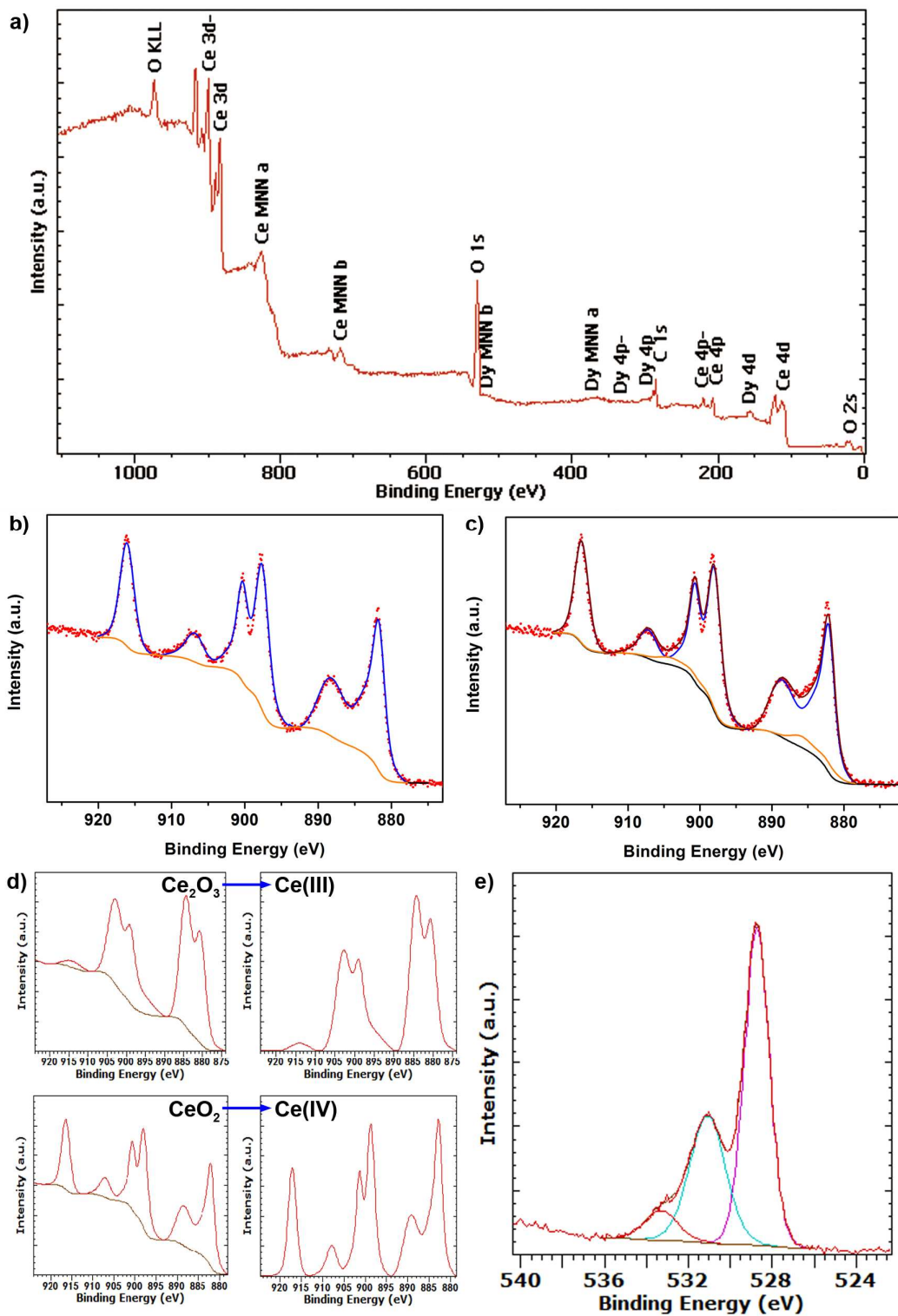


Figure S3. XPS spectra of the typical samples. a) Full spectra of CeO₂:Dy nanowires. b) Ce 3d spectra of CeO₂:Dy fitted as the linear combination of Ce(III) and Ce(IV) 3d spectra with the reported method (Ref. S4). Standard Ce(IV) and Ce(III) 3d spectra were obtained as (d) shows. c) Ce 3d spectra of undoped CeO₂ nanowires and fitting curves. (red dots: experimental data; brown line: fitted data; blue line: fitting curve for Ce(IV); orange line: fitting curve for Ce(III); black line: background). d) Ce(IV) and Ce(III) 3d spectra obtained from CeO₂ and Ce₂O₃. They were used to fit Ce 3d spectra to obtain Ce(III) proportion. e) O 1s spectra of CeO₂:Nd and peak fitting.

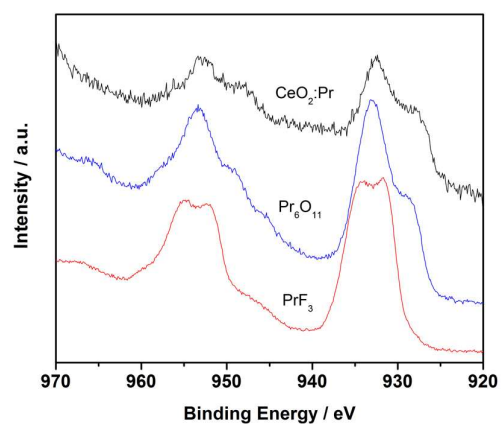


Figure S4. XPS Pr 3d spectra of CeO₂:Pr nanowires, comparing with Pr₆O₁₁. Trivalent Pr was dominant in CeO₂:Pr because the weak 3d4f¹ satellite peak at 967 eV was hardly detected (Ref. S16).

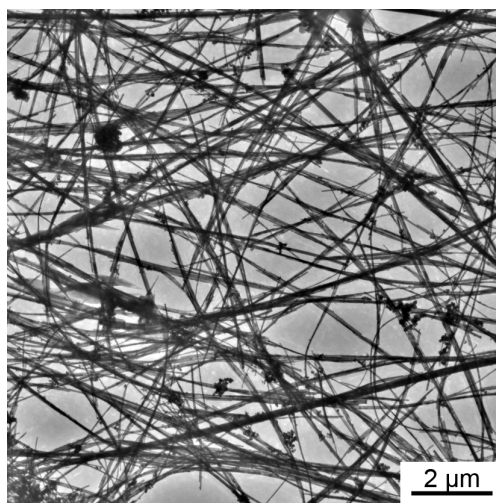


Figure S5. TEM image of undoped CeO₂ nanowires.

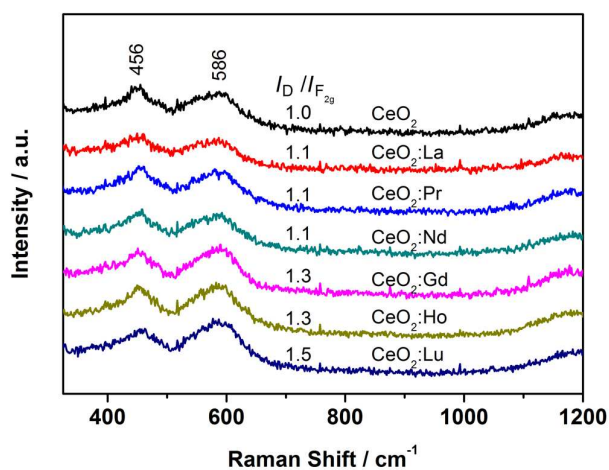


Figure S6. Raman spectra with 325 nm laser excitation for CeO₂:Ln nanowires.

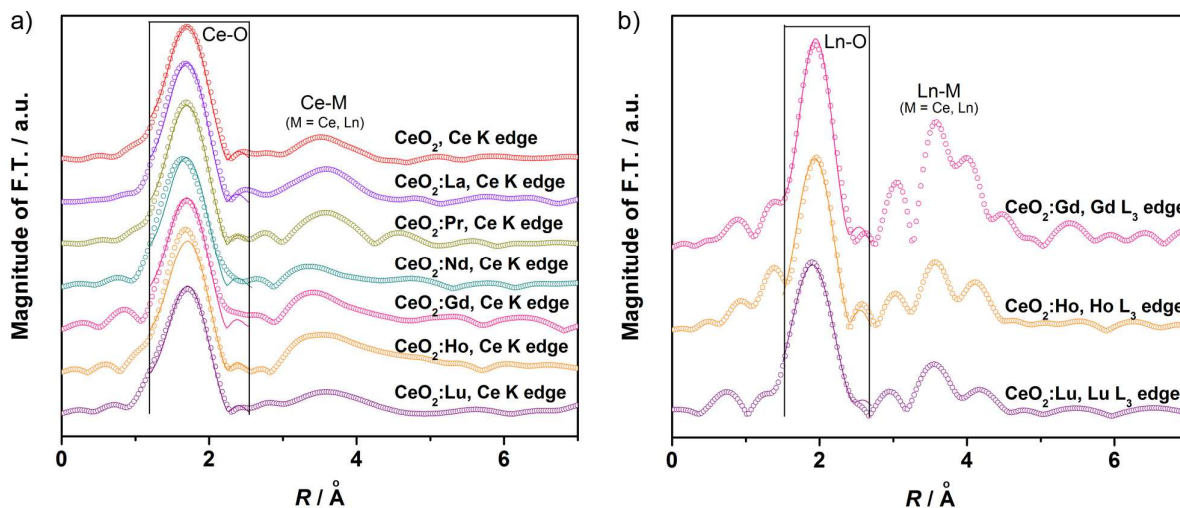


Figure S7. Fourier transforms of EXAFS spectra of undoped, Gd, Ho, and Lu doped CeO_2 nanowires and the curve fitting. Dots represent experimental data while solid lines represent fitted data. The windows represent the range in r space involved in the fitting. a) Ce K edge spectra. b) Ln L_3 edge spectra.

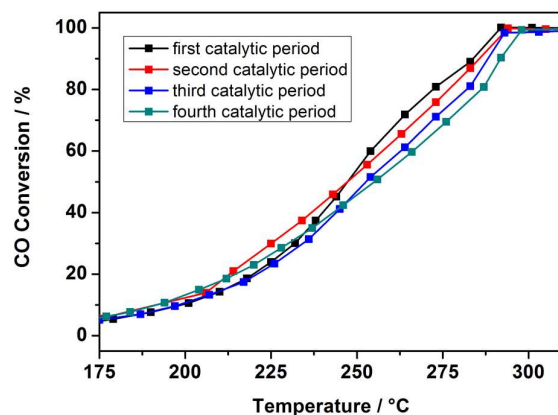


Figure S8. Light-off curves for CO conversion over CeO_2 :Nd nanowires in four continuous catalytic periods between 175 $^{\circ}\text{C}$ and 310 $^{\circ}\text{C}$.

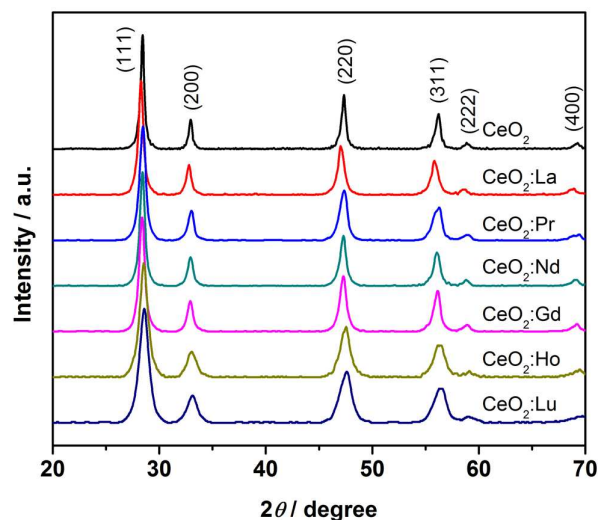


Figure S9. XRD patterns of the CeO_2 :Ln nanowires after catalysis tests. No obvious phase segregation was found after catalytic tests.

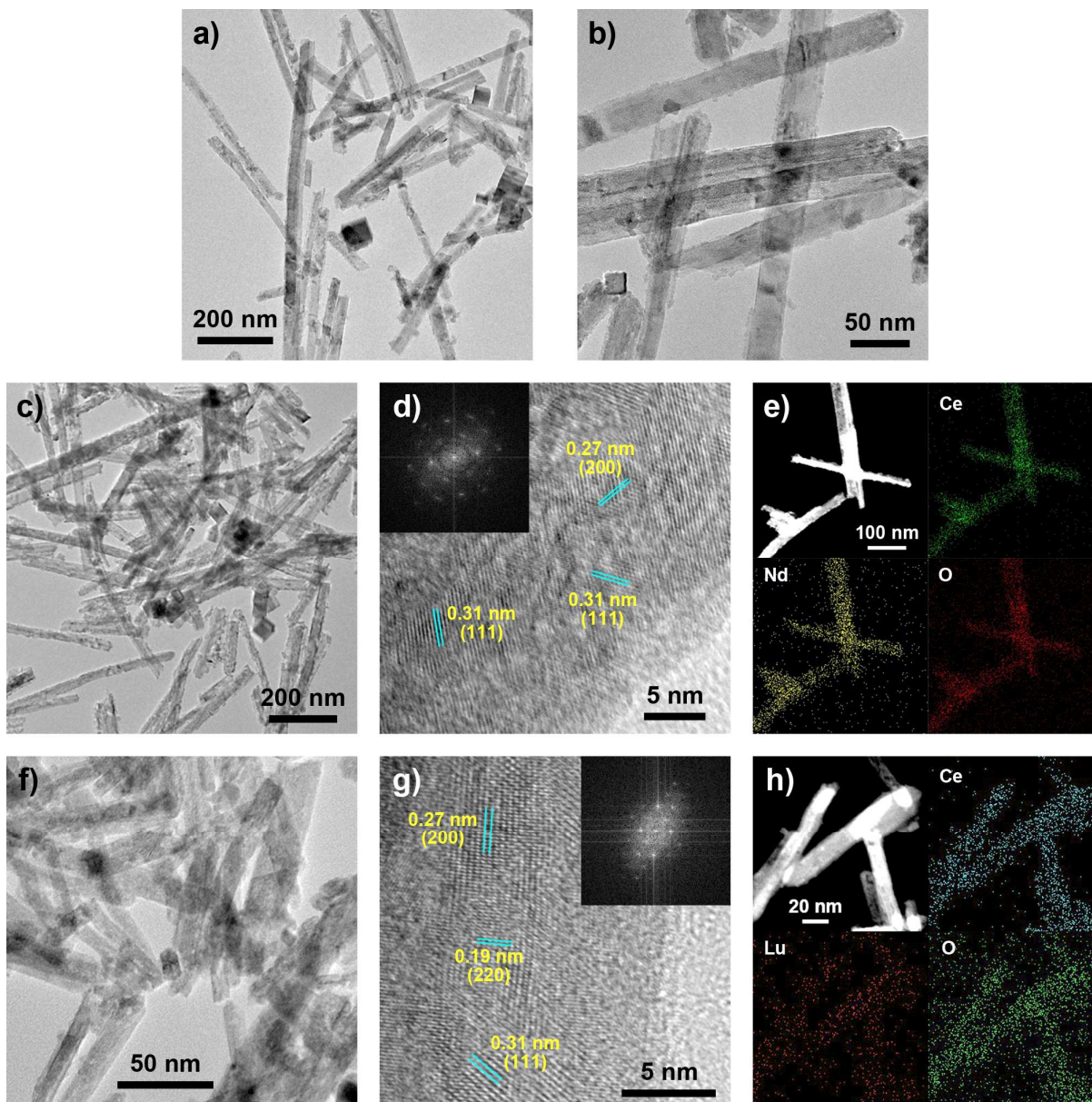


Figure S10. TEM (a–c,f), HRTEM (d,g), and HAADF-STEM EDS elemental mapping (e,h) images of undoped CeO_2 (a,b), $\text{CeO}_2\text{:Nd}$ (c–e) and $\text{CeO}_2\text{:Lu}$ nanocrystals (f–h) after catalytic tests. Insets in panel d and g are the fast Fourier transition analyses, indicating that (110) surfaces were still exposed for both samples. In panel e and h, the up-left images are the HAADF-STEM images. The up-right, bottom-left, and bottom-right images in panel e and f are the EDS elemental mapping representing Ce, O, and the dopant (Nd for panel e and Lu for panel h), respectively. The images for other $\text{CeO}_2\text{:Ln}$ samples were similar. It seems that after the catalytic reactions the nanowires sustained their morphologies while their surfaces became somewhat rough for both undoped and Ln doped samples.

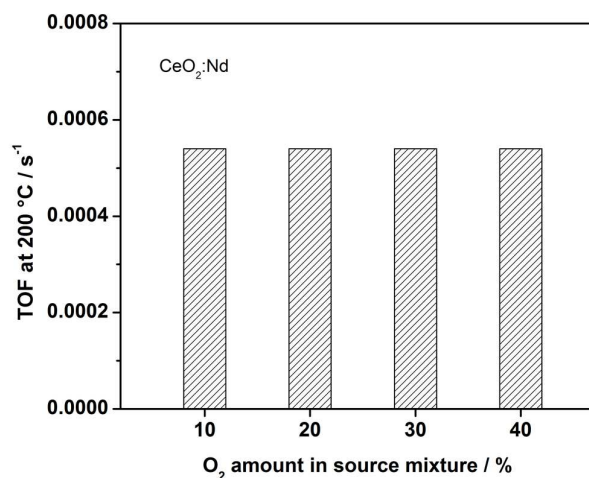


Figure S11. Variation of catalytic activity along the O₂ amount in source mixture for the typical sample CeO₂:Nd nanowires. Activity had no obvious change when the O₂ amount was doubled or halved in O₂-rich environment.

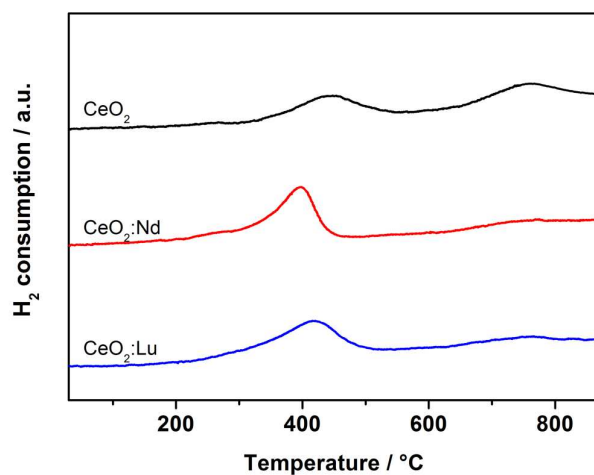


Figure S12. H₂-TPR over representative CeO₂:Ln nanowires. The peak at 650–800 °C represented the reduction of bulk ceria. Its proportion was very small for Ln doped nanowires, which was similar to the reported results (Ref. S17). A large part of the oxygen in bulk CeO₂:Ln became easier to be reduced by H₂ than that in undoped ceria because of the activation effect of the Ln³⁺ dopants and induced oxygen mobility (Ref. S17 and S18).

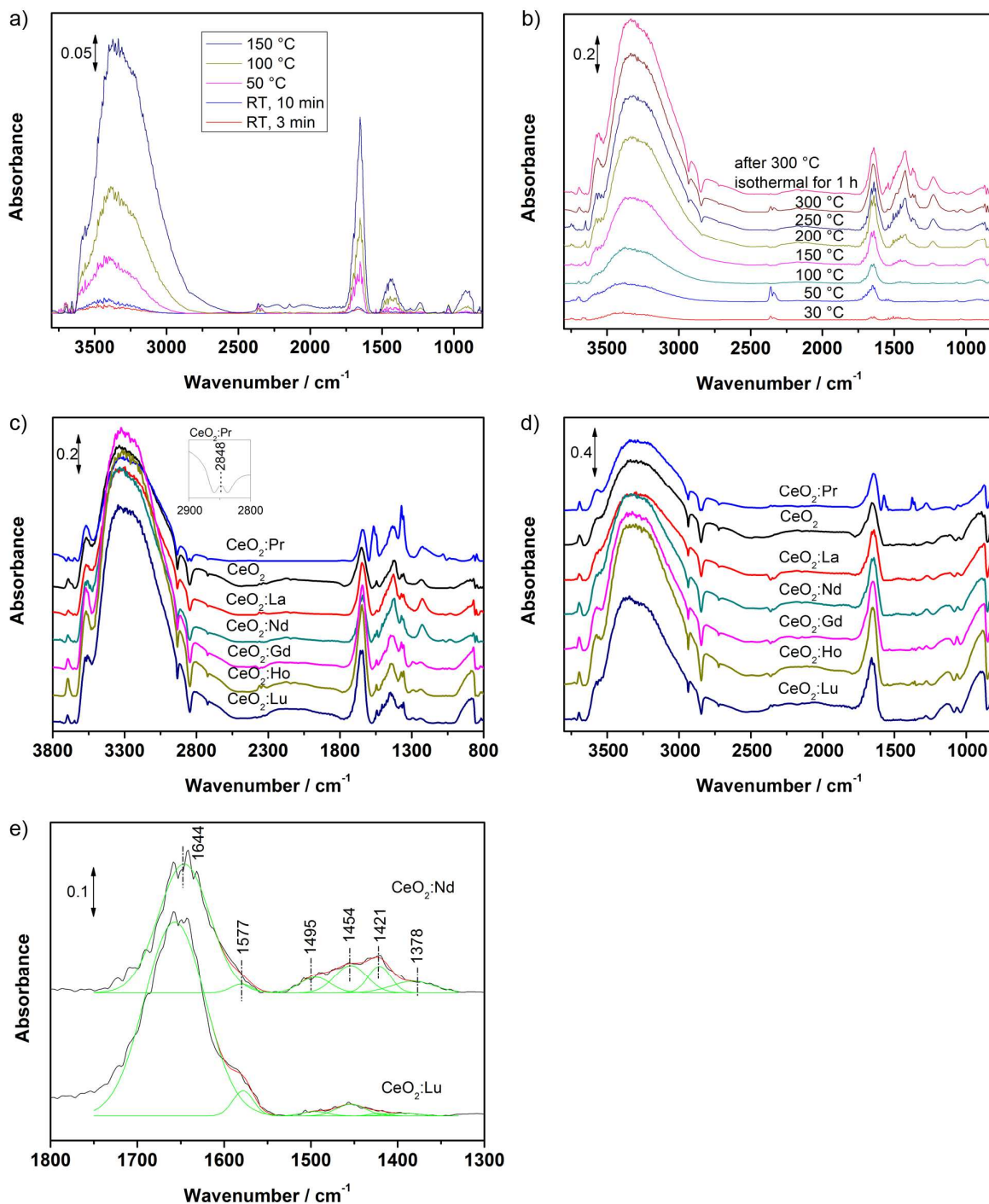


Figure S13. IR spectra for $\text{CeO}_2:\text{Ln}$ nanowires: a) CO adsorption on $\text{CeO}_2:\text{La}$ nanowires; b) CO oxidation over $\text{CeO}_2:\text{Nd}$ nanowires at varied temperatures; c) CO oxidation over $\text{CeO}_2:\text{Ln}$ nanowires at 300 °C (Insert is the enlarged figure for $\text{CeO}_2:\text{Pr}$ at selected wavenumber range); d) curves obtained under cooling down to 30 °C after the test described in panel c; e) Curve fitting with Gaussian peaks for the spectra collected during CO oxidation at 200 °C (black line, experiment data; red line, fitted data; green line, fitted peaks).

References

- Ref. S1.** Langford, J. I. *J. Appl. Crystallogr.* **1971**, *4*, 259.
- Ref. S2.** Langford, J. I. *J. Appl. Crystallogr.* **1973**, *6*, 190.
- Ref. S3.** Powell, C. J.; Jablonski, A. *NIST Electron Inelastic-Mean-Free-Path Database*, Ed. 1.2, National Institute of Standards and Technology, Gaithersburg, MD, **2010**.
- Ref. S4.** Zhang, C.; Grass, M. E.; McDaniel, A. H.; DeCaluwe, S. C.; Gabaly, F. E.; Liu, Z.; McCarty, K. F.; Farrow, R. L.; Linne, M. A.; Hussain, Z.; Jackson, G. S.; Bluhm, H.; Eichhorn, B. W. *Nature Mater.* **2010**, *9*, 944.
- Ref. S5.** Yamazaki, S.; Matsui, T.; Ohashi, T.; Arita, Y. *Solid State Ionics* **2000**, *136–137*, 913.
- Ref. S6.** Li, C.; Sakata, Y.; Arai, T.; Domen, K.; Maruya, K.; Onishi, T. *J. Chem. Soc., Faraday Trans. 1* **1989**, *85*, 929.
- Ref. S7.** Shannon, R. D. *Acta Crystallogr. Sect. A* **1976**, *32*, 751.
- Ref. S8.** Yeriskin, I.; Nolan, M. *J. Phys.: Condens. Matter* **2010**, *22*, 135004.
- Ref. S9.** Nolan, M. *J. Phys. Chem. C* **2011**, *115*, 6671.
- Ref. S10.** Santos, V. P.; Pereira, M. F. R.; Órfão, J. J. M.; Figueiredo, J. L. *Appl. Catal. B: Environ.* **2010**, *99*, 353.
- Ref. S11.** Stoch, J.; Gablankowska-Kukucz, J. *Surf. Interface Anal.* **1991**, *17*, 165.
- Ref. S12.** Mullins, D. R.; Overbury, S. H.; Huntley, D. R. *Surf. Sci.* **1998**, *409*, 307.
- Ref. S13.** Choundhury, T.; Saied, S. O.; Sullivan, J. L.; Abbot, A. M. *J. Phys. D: Appl. Phys.* **1989**, *22*, 1185.
- Ref. S14.** Jin, T.; Zhou, Y.; Mains, G. J.; White, J. M. *J. Phys. Chem.* **1987**, *91*, 5931.
- Ref. S15.** Li, C.; Sakata, Y.; Arai, T.; Domen, K.; Maruya, K.; Onishi, T. *J. Chem. Soc., Faraday Trans. 1* **1989**, *85*, 1451.
- Ref. S16.** Lütkehoff, S.; Neumann, M.; Ślebarski, A. *Phys. Rev. B* **1995**, *52*, 13808.
- Ref. S17.** Hernández, W. Y.; Laguna, O. H.; Centeno, M. A.; Odriozola, J. A. *J. Solid State Chem.* **2011**, *184*, 3014.
- Ref. S18.** Katta, L.; Sudarsanam, P.; Thrimurthulu, G.; Reddy, B. M. *Appl. Catal. B: Environ.* **2010**, *101*, 101.